Structural studies of Ni$_{2+x}$Mn$_{1-x}$Ga by powder x-ray diffraction and total energy calculations

S. Banik,[1] R. Ranjan,[2] A. Chakrabarti,[3] S. Bhardwaj,[1] N. P. Lalla,[1] A. M. Awasthi,[1] V. Sathe,[1] D. M. Phase,[1]
P. K. Mukhopadhyay,[4] D. Pandey,[2] and S. R. Barman[1],*

[1]*UGC-DAE Consortium for Scientific Research, Khandwa Road, Indore, 452017 Madhya Pradesh, India*
[2]*School of Materials Science and Technology, Banaras Hindu University, Varanasi, 221005 Uttar Pradesh, India*
[3]*Raja Ramanna Centre for Advanced Technology, Indore, 452013 Madhya Pradesh, India*
[4]*LCMP, S. N. Bose National Centre for Basic Sciences, Kolkata, 700098 West Bengal, India*

The crystal structure of Ni$_{2+x}$Mn$_{1-x}$Ga has been studied as a function of composition (x) by powder x-ray diffraction. For Ni$_{2.24}$Mn$_{0.75}$Ga, where one-fourth of the Mn atoms are replaced by Ni, the experimentally determined lattice constants are in good agreement with theoretical equilibrium lattice constants calculated by minimization of total energy using full potential linearized augmented plane-wave method. For $0.15 \leq x \leq 0.35$, a nonmodulated tetragonal martensitic phase is obtained at room temperature, whose lattice constant c increases and a decreases linearly with increasing x following Vegard's law. A 7M modulated monoclinic phase is obtained for $x=0.2$ due to annealing. The small width of the hysteresis of the martensitic transition shows its thermoelastic nature that is the characteristic of a shape memory alloy. Phase coexistence is observed for $0.1 \leq x \leq 0.15$ at room temperature, confirming the first-order nature of the martensitic transition.

I. INTRODUCTION

Ni$_2$MnGa is a ferromagnetic Heusler alloy, which is of immense recent interest because it exhibits shape memory effect (SME) that can be driven by the magnetic field. This makes it an important candidate for practical applications, since the response in magnetic-field-driven shape memory alloy is faster and is more efficient than the conventional SME driven by temperature or stress.[1,2] Ni-Mn-Ga exhibits the highest known magnetic-field-induced strain of up to 10%. Giant magnetocaloric effect and large negative magnetoresistance have also been reported for these alloys.[3–5] Thus, different technological applications such as actuators, sensors, robotics, magnetic refrigeration, and medical use are being envisaged.[1,2,4]

The martensitic transition in Ni$_2$MnGa was first reported by Webster *et al.* in 1984.[6] Ni$_2$MnGa has an $L2_1$ structure at room temperature. The structural transition is characterized by the martensitic start temperature (T_M=202 K), in which the parent ferromagnetic cubic (austenitic) phase transforms to the martensitic phase with modulated orthorhombic structure.[7] The paramagnetic to ferromagnetic Curie transition occurs at T_C=376 K, which is above T_M. In the nonstoichiometric compositions like Ni$_{2+x}$Mn$_{1-x}$Ga, the martensitic and magnetic transition temperatures, magnetocrystalline anisotropy, enthalpy, and saturation magnetization are highly sensitive to the composition.[8–10] The substitution of Mn with Ni results in the increase of T_M and decrease of T_C with increasing x. For the compositions with x greater than 0.2, T_M is larger than T_C.[11,12]

Depending on composition, the Ni-Mn-Ga martensitic phases have been reported to assume complicated monoclinic or tetragonal structure with 5M modulation or orthorhombic structure with 7M modulation.[2,6,7,13–15] The 7M (5M) phase corresponds to seven-layer (five-layer) modulation of the (110) planes in $[1\bar{1}0]$ direction in the austenitic phase. From a Rietveld analysis of the neutron and x-ray powder diffraction data, Brown *et al.* and Ranjan *et al.* have shown that Ni$_2$MnGa in the martensitic phase has a 7M orthorhombic structure in the *Pnnm* space group.[7,16] However, a tetragonal phase that does not exhibit any modulation has been reported for nonstoichiometric Ni-Mn-Ga with Ga deficiency and Ni and Mn excess.[13,14]

Ni$_2$MnGa has been studied theoretically by different groups.[17–22] Godlevsky and Rabe, using local spin-density pseudopotential calculations, obtained the total energy (E_{tot}) minimum at c/a=1, with other shallow local minima at 1.08 and 1.2.[17] On the other hand, Ayuela *et al.* reported the E_{tot} minimum around c/a=1.25 and claimed existence of a local minimum around 0.94.[20] We have recently shown that the martensitic phase, which occurs at lower temperature and is hence expected to be energetically more stable, indeed has lower energy compared to the austenitic phase.[22] The c/a value is in good agreement with the experimental value of 0.94.[6,26] However, there are very few studies on nonstoichiometric Ni$_{2+x}$Mn$_{1-x}$Ga,[27,28] possibly because of the increase in computational complexity. MacLaren calculated the density of states (DOS) for 20% Ni-rich Ni$_2$MnGa using layer Korringa-Kohn-Rostocker method and correlated the structural properties with DOS.[27] By comparing the photoemission valence-band spectra with the calculated density of states of Ni$_{2.25}$Mn$_{0.75}$Ga, evidence of Ni clustering and decrease in minority-spin DOS near E_F have been found.[28]

The crystal structure and the c/a ratio, in particular, influence both the magnetic and mechanical properties of Ni$_{2+x}$Mn$_{1-x}$Ga. In fact, the magnetic-field-induced strain is related to $(c/a-1)$.[14] The phenomenological magnetoelastic model for Ni$_2$MnGa ferromagnetic shape memory alloy[23] and *ab initio* calculations[24] predict a linear dependence of the magnetic anisotropy parameter of Ni-Mn-Ga on the spontaneous strain ϵ_{ii}, which is proportional to $(c/a-1)$. Moreover, the magnetocrystalline anisotropy is reported to decrease with increase in c/a ratio.[9,25] Thus, the differences in the martensitic transition temperatures and the magnetoelastic

properties in the Ni-Mn-Ga system are related to the difference in the crystal structure of the martensitic phase. In a rigid band picture, the shift of the Fermi level is related to e/a, where e/a is the ratio of valence electron concentration per atom. Although the variation of c/a as a function of e/a for different Ni-Mn-Ga compositions has been reported,[14] to the best of our knowledge, no study of the $Ni_{2+x}Mn_{1-x}Ga$ structure as a function of x exists in literature. The present work is devoted to a detailed investigation of the crystal structures and lattice-constant variation of $Ni_{2+x}Mn_{1-x}Ga$ in the composition range $0 \leq x \leq 0.35$ using powder x-ray diffraction. All-electron *ab initio* full potential linearized augmented plane-wave (FPLAPW) method has been employed to determine the equilibrium structure of $x=0.25$ in both the martensitic and austenitic phases. In Sec. III A, we determine the lattice parameters for $Ni_{2.24}Mn_{0.75}Ga_{1.02}$ (referred to henceforth as $Ni_{2.24}Mn_{0.75}Ga$ or $x=0.24$) by Rietveld analysis of the x-ray diffraction (XRD) data and then compare them with the equilibrium theoretical lattice parameters for $Ni_{2.25}Mn_{0.75}Ga$ using FPLAPW. The agreement is very good. Sec. III B deals with the variation of lattice parameters as a function of composition at room temperature within the martensitic ferromagnetic tetragonal phase, while in Sec. III C, we study the structural changes that are induced by thermal treatment. Section III D deals with the phase coexistence in the composition range of $0.1 \leq x \leq 0.15$.

II. METHODS: EXPERIMENT AND THEORY

Polycrystalline ingots of $Ni_{2+x}Mn_{1-x}Ga$ were prepared by arc melting the appropriate quantities of the constituent metals of 99.99% purity under argon atmosphere. The subsequent homogenization of the ingot material was carried out by annealing at 827 °C for nine days in sealed quartz ampules. The samples were subsequently quenched in ice water. Since the properties of $Ni_{2+x}Mn_{1-x}Ga$ are highly composition dependent, the composition has been determined by energy dispersive analysis of x-rays (EDAX) using JEOL JSM 5600 scanning electron microscope with Oxford detector model No. 6587. EDAX has been performed by estimating the intensities of Ni, Mn, and Ga $K\alpha$ characteristic lines (5.9–9.2 keV) that are well separated and have small background by averaging over several measurements on the same specimen with 2% accuracy.

The powder XRD data at room temperature (293 K) were obtained with Cu $K\alpha$ radiation using a Rigaku x-ray diffractometer (RUH3R). The data were recorded at the rate of 2°/min with a step size of 0.02°. For XRD, pieces cut from the ingot were manually ground into powder. Internal residual stress was removed by annealing the powder at 500 °C for 10 h. Structure refinement was carried out by Rietveld method using the DBWS-9411 software.[29] Differential scanning calorimetry (DSC) was done by using TA Instruments MDSC model 2910 at a scan rate of 10°/min. The temperature-dependent low-field χ_{ac} measurements were carried out using an ac susceptometer at 26.6 Oe rms field and 33.33 Hz frequency.

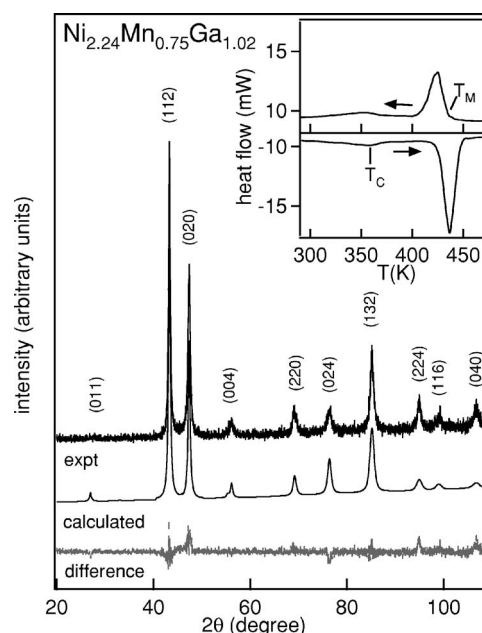The *ab initio*, relativistic, and spin-polarized FPLAPW calculations were performed using the WIEN97 code.[30] Gen-

FIG. 1. X-ray diffraction (XRD) pattern of $Ni_{2.24}Mn_{0.75}Ga$ ($x=0.24$). The calculated and difference profiles are also shown. The indices are with respect to the body-centered tetragonal ($I4/mmm$) cell (see text). The inset shows the exothermic and endothermic heat flows; arrows indicate the heating and cooling directions.

eralized gradient approximation (GGA) was used for the exchange correlation.[31] The cutoff for charge density was $G_{max}=14$. The muffin-tin (MT) radii were taken to be as follows: Ni, 2.012 a.u.; Mn, 2.1472 a.u.; and Ga, 2.012 a.u. The parameters used were as follows: $R_{MT}K_{max}=8.5$, $l_{max}=10$, $l_{max,ns}=4$, and $G_{max}=14$. 2200 k points were taken in the Brillouin zone for self-consistent field cycles. All the other parameters were kept at the default values generated by the WIEN97 code. The calculations were performed with the convergence criterion for E_{tot} to be 0.1 mRy, i.e., with an accuracy of ±0.085 meV/atom, as in our recent work on Ni_2MnGa.[22] The equilibrium lattice constants have been determined by the standard method of minimizing E_{tot}.[30] E_{tot} consists of the total kinetic, potential, and exchange-correlation energies of a periodic solid with frozen nuclei.[32] For the tetragonal martensitic phase, E_{tot} has been calculated as a function of c/a for the experimental unit-cell volume. In the case of the cubic austenitic phase, E_{tot} has been minimized as a function of a.

III. RESULTS AND DISCUSSION

A. Structure of $Ni_{2.24}Mn_{0.75}Ga$: Comparison of XRD and FPLAPW results

The XRD pattern of $Ni_{2.24}Mn_{0.75}Ga$ at room temperature (293 K) is characteristic of a tetragonal distortion of the cubic austenite cell. All the peaks in the pattern can be indexed by a tetragonal $I4/mmm$ unit cell. The (022) reflection of the cubic austenitic cell (as will be shown later in Fig. 5 for $x=0.01$) is split into two peaks around $2\theta=43.3°$, whose indices are (112) and (020) (Fig. 1). No reflections in the XRD
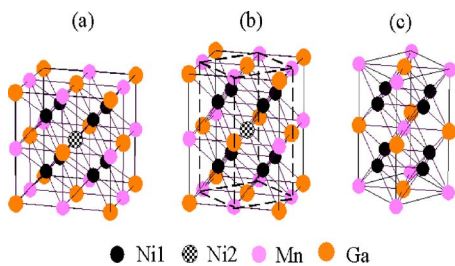
FIG. 2. (Color online) (a) The unit cell of Ni$_{2.24}$Mn$_{0.75}$Ga in the austenitic cubic phase, (b) the face-centered (*F*) unit cell, and (c) the body-centered (*I*) unit cell in the martensitic phase. The body centered unit cell is shown by dashed lines in (b). The Ni atom that replaces Mn is referred to as Ni2, while the Ni atoms in Ni positions are indicated by Ni1.

pattern that indicate the presence of 7*M* modulation in the sample have been observed, unlike for the stoichiometric composition, Ni$_2$MnGa.[6,7,15,16] The absence of modulation in Ni$_{2.24}$Mn$_{0.75}$Ga is supported by previous structural and theoretical studies, where it was found that modulation is absent for Ni-Mn-Ga compositions with $c/a > 1$.[13,14,21]

The tetragonally distorted martensite has been described in literature by the tetragonal space group *I*4/*mmm* ($Z=2$) and also by the orthorhombic *Fmmm* space group ($Z=4$) with $a=b$.[6,26] However, the constraint $a=b$ transforms the *Fmmm* space group into the higher symmetry *I*4/*mmm* space group, which is therefore the correct space group. Rietveld refinement was therefore performed using the *I*4/*mmm* space group. All the atoms occupy fixed high-symmetry special positions. The Wyckoff positions of the different atoms are as follows: Ni1: (4*d*) 0, 0.5, 0.25; Mn: (2*b*) 0, 0, 0.5; Ga: (2*a*) 0, 0, 0; and Ni2: (2*b*) 0, 0, 0.5, where Ni1 is the Ni atom at Ni position and Ni2 is the extra Ni (0.25) at Mn position. Pseudo-Voigt profile function was selected to model the line shapes of the various Bragg reflections. During the refinement, scale factor, zero correction, shape parameters, half-width parameters, lattice parameters, and isotropic thermal parameters were varied. Figure 1 depicts the observed, calculated, and difference plots obtained after the Rietveld refinement. There is good agreement between the observed and the calculated profiles. The goodness of fit is 1.2, suggesting the correctness of the structural model. The refined cell parameters are $a_I = 3.846 \pm 0.001$ Å and $c_I = 6.563 \pm 0.001$ Å, where *I* stands for the body-centered unit cell [Fig. 2(c)]. However, for ease of comparison of the unit cells of the austenite and martensite phases, as is evident from Fig. 2, we express the lattice constants in terms of a larger 16-atom face-centered unit cell [Fig. 2(b)] rather than the smaller conventional cell for the *I*4/*mmm* space group shown in Fig. 2(c). The lattice constants of the body-centered (*I*) and face-centered (*F*) unit cells for the *I*4/*mmm* space group are related by $a=a_F=\sqrt{2}a_I$ and $c=c_F=c_I$. Thus, the lattice constants of Ni$_{2.24}$Mn$_{0.75}$Ga turn out to be $a=5.439$ Å (10.282 a.u.) and $c=6.563$ Å (12.406 a.u.), with c/a ratio of 1.21.

In our refinement, we have assumed that the excess Ni (Ni2) atoms occupy the Mn sites because equivalent number of Mn sites would be vacant, as is evident from the compo-

sition Ni$_{2+x}$Mn$_{1-x}$Ga. This is supported by photoemission experiments and DOS calculations using FPLAPW, which show that Ni2 occupies predominantly the Mn position. Extra states in valence band and DOS appear due to bonding between 3*d* states of Ni1 and Ni2 that are nearest neighbors (Fig. 2).[28] These states can appear in the DOS only if Ni2 is in the Mn position and are absent if Ga occupies Mn sites. We also considered other possibilities in the refinement, for example, Ni2 replacing Ga and the replaced Ga occupying Mn sites, and antisite defects, i.e., exchange of Ni and Mn atom positions. The goodness of fit and the lattice constants remain similar in all these cases, showing that the lattice parameter is not influenced by these defects. On the other hand, the possibility of the existence of these defects cannot be ruled out based on our XRD analysis. However, such defects have been shown to be small in Ni-Mn-Ga from neutron-diffraction measurements.[7,33]

DSC results confirm that Ni$_{2.24}$Mn$_{0.75}$Ga is indeed martensitic at RT (inset, Fig. 1). T_M and martensitic finish (T_{M_f}) temperatures are 434 and 408 K, respectively. The austenitic start (T_{A_s}) and finish (T_{A_f}) temperatures are 423 and 447 K, respectively. The weak feature around 350 K ($=T_C$) in both the heating and cooling curves is related to the second-order ferromagnetic to paramagnetic transition. Hence, clearly in this case the martensitic transition temperatures are well above T_C and occur in the paramagnetic state. Recently, Khovaylo *et al.* have reported the existence of coupled magnetostructural transition ($T_M=T_C$) between $x=0.2$ and 0.27.[11] This is in disagreement with our result for $x=0.24$, and this might be related to the uncertainty in the determination of the composition. Since the properties are highly composition sensitive, we have carefully determined the compositions by EDAX, while Khovailo *et al.* did not report any such compositional analysis.[11,12] Alternatively, the discrepancy could also be partly due to the history of the sample preparation.

We have calculated the equilibrium lattice constants of Ni$_{2.25}$Mn$_{0.75}$Ga by minimizing the total energy using the FPLAPW method. For the martensitic phase that is ferromagnetic and tetragonal (FT), we have used the atomic positions of the bigger face-centered cell containing four formula units [see Fig. 2(b)]. The Ni2 atom was assumed to occupy one of the four Mn sites in the calculations. The total energy (E_{tot}) has been minimized as a function of c/a between 0.88 and 1.4, keeping the unit-cell volume fixed at the experimental value [Fig. 3(a)]. E_{tot} values are given in a relative scale assuming the lowest-energy value to be zero. We find the c/a corresponding to minimum E_{tot} by fitting the data between $c/a=1.05$ and 1.4 using the Murunagan fitting scheme.[34] Minimum E_{tot} is obtained at $c/a=1.245 \pm 0.005$. The corresponding equilibrium lattice constants turn out to be $a=10.17$ a.u. (5.38 Å) and $c=12.67$ a.u. (6.70 Å). Between $c/a=0.93$ and 1.05, a shallow local minimum in E_{tot} is observed at 0.95, and a similar local minimum in E_{tot} has been reported earlier for Ni$_2$MnGa.[17,22] Absence of any global minimum in this region is in contrast to Ni$_2$MnGa, where E_{tot} minimum has been observed at $c/a=0.97$ with $a=11.11$ a.u. (5.88 Å) and $c=10.78$ a.u. (5.70 Å).[22] Comparison of the lattice constants of Ni$_{2.25}$Mn$_{0.75}$Ga and Ni$_2$MnGa show that there is a sizable elongation along the *c* axis (17%)
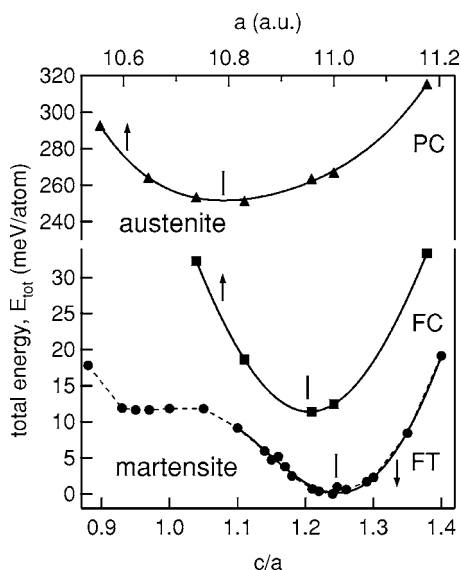
FIG. 3. The total energy (E_{tot}) of $Ni_{2.25}Mn_{0.75}Ga$ ($x=0.25$) in the martensitic ferromagnetic tetragonal (FT) phase as a function of c/a, and austenitic ferromagnetic cubic (FC) and paramagnetic cubic (PC) phases as a function of a. The solid lines are the fitted curve, the dashed line joins the data points for FT phase. The arrows indicate the axis with respect to which the data are plotted and the bold ticks show the minimum E_{tot} position.

and a contraction along a and b axes by 8.3%. The unit-cell volume of $Ni_{2.25}Mn_{0.75}Ga$ is, however, contracted by 0.35% only with respect to that of Ni_2MnGa. For Heusler alloys, GGA accounts for the density gradients and provides a better overall agreement with experiment compared to local-density approximation.[35,36] The agreement between the experimental and theoretical lattice constants in the martensitic phase (expt.: $a=5.439$ Å, $c=6.563$ Å; theory: $a=5.38$ Å, $c=6.70$ Å) for $Ni_{2.25}Mn_{0.75}Ga$ is within 1% for a and 2% for c. In the case of Ni_2MnGa, a and c values are obtained within 0.7% and 2.5% of the experimental values using GGA approximation.[22] For sake of comparison, we may mention that the difference in the lattice parameters of Fe obtained by GGA based density-functional theory and the experimental value is 3.5%.[37] Similarly, for free-electron-like nonmagnetic metals (Na, Li), the discrepancy in lattice constants is in the range of 0.1%–2%.[38] Considering that $Ni_{2.25}Mn_{0.75}Ga$ has a site disorder related to the doped Ni atoms that is not accounted for in the theory, the agreement between experiment and theory obtained here might be considered to be good. This also shows that disorder has a small influence on the structural parameters. Moreover, the good agreement also indicates that the variation of lattice constants between room and low temperature is small, since all the calculations are for ground state at absolute zero, while the lattice constants have been measured at room temperature. Recent temperature-dependent measurements of the lattice constants for near stoichiometric $Ni_2Mn_{0.95}Ga_{0.95}$ indeed show that their variation is less than 1% between 15 and 210 K.[16] It should be noted that we obtained a ferromagnetic ground state for $Ni_{2.25}Mn_{0.75}Ga$ with the total magnetic moment of $3.28\mu_B$, while experimental saturation magnetic moment from Compton scattering is $2.73\mu_B$.[39]
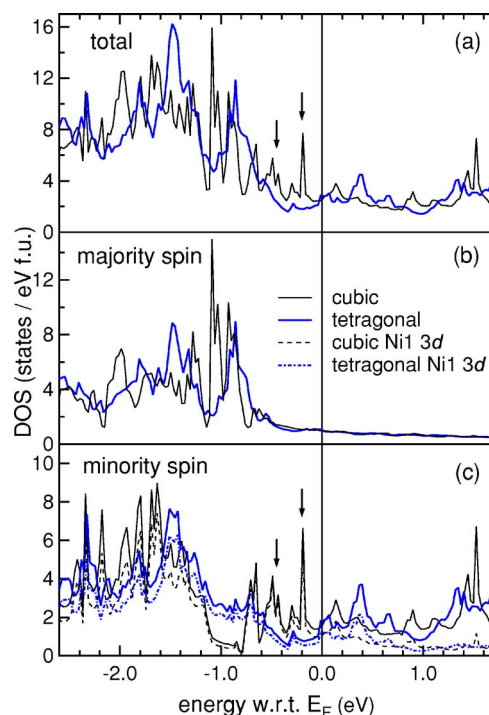

FIG. 4. (Color online) (a) Total and (b) majority- and (c) minority-spin DOS and Ni $3d$ PDOS of $Ni_{2.25}Mn_{0.75}Ga$ in the equilibrium tetragonal structure with $c/a=1.245$ and the cubic phase with $c/a=1$.

The stabilization of the tetragonally distorted martensitic phase in Ni_2MnGa has been explained by Fujii *et al.* to be related to band Jahn-Teller effect.[18] Using the Korringa-Kohn-Rostocker method, they showed that a DOS peak at E_F in the cubic phase splits into two peaks below and above E_F in the tetragonal phase, resulting in a lowering of the total energy. To understand the stabilization of the tetragonal martensitic phase of $Ni_{2.25}Mn_{0.75}Ga$ (with $c/a=1.245$) compared to the cubic structure with $c/a=1$, we show the spin-polarized DOS in Fig. 4. The total DOS is dominated by Ni $3d$-Mn $3d$ hybridized states centered around -1.5 eV [Fig. 4(a)]. The DOS peak above E_F at 1.5 eV arises primarily from the minority spin Mn $3d$ states.[22] Interesting differences are observed between E_F (=0 eV) and -0.7 eV in the minority-spin DOS [Fig. 4(c)]: the states giving rise to the peaks at -0.2 and -0.5 eV (shown by arrows) in the cubic structure are shifted to lower energies below -0.7 eV in the tetragonal structure. These peaks arise primarily from Ni1 $3d$ minority-spin states, as shown in Fig. 4(c). Orbital analysis shows that the dominant (80%) contribution is from Ni1 $3d$ t_{2g} states, with small admixture of Ni1 $3d$ e_g states. The peak just above E_F at 0.15 eV, which also arises from the Ni1 $3d$ t_{2g} states, shifts to 0.35 eV in the tetragonal structure. Thus, we may conclude that a possible reason for the stability of the tetragonal structure could be the splitting of the Ni1 $3d$ t_{2g} states around E_F.

The equilibrium lattice constants (a) for the austenitic phase in the ferromagnetic cubic (FC) and paramagnetic cubic (PC) phases have been determined by minimizing E_{tot} as a function of a (Fig. 3, top two curves). Considering first the paramagnetic phase, which has been identified

TABLE I. Composition, x, e/a ratio, lattice constants at room temperature, martensitic start temperature (T_M), Curie temperature (T_C), space group, and goodness of fit (S) for the Rietveld fitting for various specimens of Ni$_{2+x}$Mn$_{1-x}$Ga. Note that only structural studies have been done for the compositions $x=0.07$, 0.15, and 0.26. The error in determining the lattice parameters vary from ±0.0005 to ±0.0015.

Composition	x	e/a	a (Å)	c (Å)	T_M (K)	T_C (K)	Space group	Goodness of fit (S)
Ni$_2$Mn$_{1.05}$Ga$_{0.95}$	0	7.463	5.820	5.820	207	360	$Fm\bar{3}m$	1.15
Ni$_{2.01}$Mn$_{0.99}$Ga	0.01	7.508	5.820	5.820	205	365	$Fm\bar{3}m$	1.26
Ni$_{2.03}$Mn$_{0.96}$Ga	0.03	7.513	5.821	5.821	205	376	$Fm\bar{3}m$	1.30
Ni$_{2.07}$Mn$_{0.91}$Ga$_{1.02}$	0.07	7.533	5.826	5.826			$Fm\bar{3}m$	1.28
Ni$_{2.1}$Mn$_{0.9}$Ga	0.1	7.575	5.813	5.813	276	344	$Fm\bar{3}m$, $I4/mmm$	1.24
Ni$_{2.13}$Mn$_{0.87}$Ga$_{1.02}$	0.13	7.613	5.811	5.811	292	339	$Fm\bar{3}m$, $I4/mmm$	1.17
Ni$_{2.15}$Mn$_{0.84}$Ga	0.15	7.603	5.795, 5.501	5.795, 6.469			$Fm\bar{3}m$, $I4/mmm$	1.26
Ni$_{2.19}$Mn$_{0.82}$Ga	0.19	7.653	5.494	6.484	329	331	$I4/mmm$	1.30
Ni$_{2.20}$Mn$_{0.8}$Ga	0.2	7.650	5.482	6.488	334	334	$I4/mmm$	1.24
Ni$_{2.24}$Mn$_{0.75}$Ga$_{1.02}$	0.24	7.678	5.439	6.563	434	351	$I4/mmm$	1.21
Ni$_{2.26}$Mn$_{0.73}$Ga$_{1.02}$	0.26	7.693	5.440	6.566			$I4/mmm$	1.18
Ni$_{2.32}$Mn$_{0.67}$Ga$_{1.02}$	0.32	7.738	5.422	6.605	508	331	$I4/mmm$	1.30
Ni$_{2.35}$Mn$_{0.66}$Ga$_{0.98}$	0.35	7.765	5.404	6.649	537	320	$I4/mmm$	1.21

experimentally,[12] we find that E_{tot} minimum of the PC phase is 253 meV/atom higher than the E_{tot} minimum of the martensitic phase. This energy difference is in agreement with that obtained in Ref. 12 ($39+210=249$ meV/atom), where the E_{tot} has been calculated using the experimental lattice constants. The reason for higher energy of the paramagnetic phase has been related to reduced hybridization between the Ni and Mn 3d states.[12,19] For the FC phase, E_{tot} minimum is higher by 11.4 meV/atom than that of the FT phase. The equilibrium lattice constant is $a=10.95$ a.u. (5.80 Å) in the FC phase, while it is somewhat smaller in the PC phase: 10.79 a.u. (5.71 Å). The lattice constant for the austenitic phase that exists above 434 K (see Table I) has not been reported in literature. However, the calculated a for Ni$_{2.25}$Mn$_{0.75}$Ga FC phase is close to $a=5.81$ and 5.82 Å for Ni$_2$MnGa FC phase obtained from theory[22] and XRD, respectively. Thus, in the austenitic phase, the lattice constant is less sensitive to x.

B. Structural variation of Ni$_{2+x}$Mn$_{1-x}$Ga with composition

Room-temperature XRD profiles for Ni$_{2+x}$Mn$_{1-x}$Ga for different x along with the calculated and difference profiles obtained by Rietveld analysis of the XRD data are shown in Fig. 5. The agreement between the observed and calculated profiles are quite satisfactory, as shown by the difference profiles and the goodness of fit (S) values. All the peaks can be indexed and the intensities of the peaks can be simulated with the space groups used. For $x=0.01$, the XRD pattern can be indexed with the cubic $L2_1$ structure with $Fm\bar{3}m$ space group, since at room temperature it is in the austenitic phase. For $x=0.13$, the emergence of a peak at 43.2° indicates the appearance of a tetragonal martensitic phase with $I4/mmm$ space group. Table I shows the compositions, lattice param-

eters, T_M, T_C, space groups used for the Rietveld analysis, and the goodness of fit (S).

A close look at the XRD patterns in Fig. 5 indicates a systematic change of the lattice constants in the martensitic
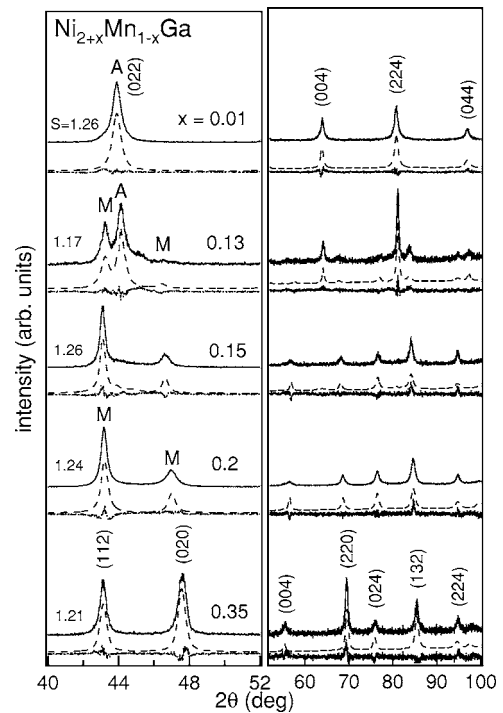

FIG. 5. X-ray diffraction pattern (solid line) of Ni$_{2+x}$Mn$_{1-x}$Ga for different x at room temperature. The calculated profiles obtained by Rietveld refinement (dashed lines) and the difference profiles are shifted along the vertical axis for clarity of presentation. A and M indicate the austenitic and martensitic phases, respectively. The panel on the right side is multiplied by 5.
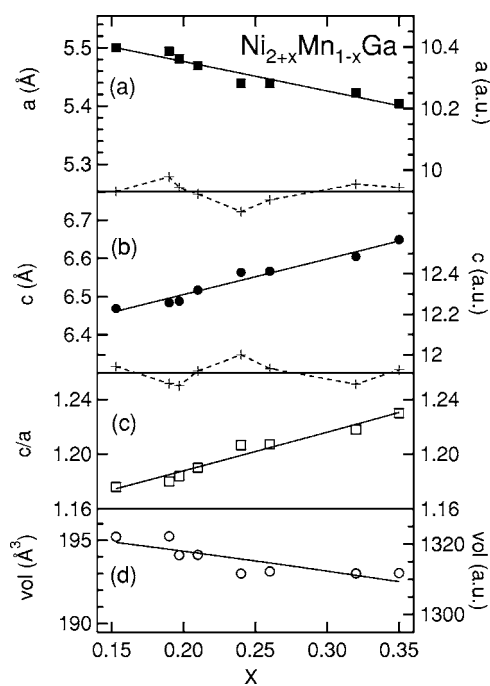
FIG. 6. Lattice parameters (a,c), c/a ratio, and the unit-cell volume of $Ni_{2+x}Mn_{1-x}Ga$ for $0.15 \leq x \leq 0.35$ in the martensitic phase at room temperature. Straight lines (solid line) have been fitted to $a(x)$ and $c(x)$. Lines through c/a and unit-cell volume are derived from the straight lines fitted to a and c.

phase. For example, for $x \geq 0.15$, the separation between the (112) and (020) peaks increases gradually with increasing x from 3.5° to 3.6°. a, c, c/a ratio, and the unit-cell volume obtained by the Rietveld fitting of the XRD patterns are shown in Fig. 6. Between $x=0.15$ and 0.35, the unit cell is elongated along the c direction by 2.7% and compressed along the a and b axes by 1.75% with increasing x. The increase in c/a ratio increases the transformation strain due to the lattice distortion. The spontaneous strain, given by $(c/a-1)$, increases from 17.6% to 23% between $x=0.15$ and 0.35. There is a small decrease by about 0.8% in the unit-cell volume, since the decrease in a and b is not fully compensated by the increase in c.

Straight line fit to the data shows that a and c vary linearly with x [Figs. 6(a) and 6(b)]. Linear variation of lattice constants in alloys can be explained by Vegard's law, which states that in the absence of strong electronic effects, the variation of the lattice parameters is linear with composition in a true three-dimensional solid solution.[40] This is a consequence of the way a solid solution reduces strain by expansion or by compression when atoms of different sizes are involved. Denton and Ashcroft provided a theoretical basis to Vegard's law by applying density-functional theory to random binary alloy systems to show that the linear variation of lattice constant is expected if the ratio of the atomic radii is sufficiently close to unity.[41] Linear variation of lattice constants with composition has been observed in many systems such as metallic solid solutions,[42] diluted magnetic semiconductors,[43] and quaternary semiconductors.[44] For $Ni_{2+x}Mn_{1-x}Ga$, both a and c do not exhibit any systematic deviation from the straight line, as is evident from the resi-

due of the linear fit. Thus, Vegard's law is obeyed over the composition range of $0.15 \leq x \leq 0.35$. This is expected because both Ni and Mn are $3d$ elements with similar electronic configuration and small size difference; the atomic radii of Ni and Mn are reported in literature to be 1.35 and 1.40 Å, respectively, and their ratio is close to 1 (0.96). The compositions prepared by us for higher x, such as $x=0.5$, have not been considered because they exhibit the presence of an additional $L1_2$ phase corresponding to Ni_3Ga.

A scrutiny of the literature for lattice parameters with compositions similar to ours reveals good agreement with previous studies.[13,45–47] For example, Pons *et al.* show that the lattice constants of $Ni_{58.3}Mn_{15.9}Ga_{25.8}$ ($Ni_{2.332}Mn_{0.64}Ga_{1.03}$) are $a=7.6$ Å and $c=6.54$ Å.[13] Their a value appears to be different from what we report for a very similar composition $Ni_{2.32}Mn_{0.67}Ga$ ($a=5.422$ Å, $c=6.605$ Å). However, this apparent disagreement arises because they use a bigger unit cell ($L1_0$), while we have used $L2_1$. For comparison, their a needs to be divided by $\sqrt{2}$, giving $a=5.375$ Å that is close to our value.

The variation of T_C and T_M for different compositions is given in Table I. Between $x=0$ and 0.2, our data are in agreement with Vasilev *et al.*, where T_C decreases and T_M increases with x before they merge at around 0.2. For $x>0.2$, T_M continues to increase while T_C decreases, and thus T_M becomes larger than T_C. This means that the martensitic transition occurs in the paramagnetic phase.[11,12]

C. Structural modifications due to annealing

For the stoichiometric Ni_2MnGa, a 7-layer modulation ($7M$) of the structure has been reported.[6,7,15,16] However, structural and theoretical studies on various nonstoichiometric compositions of Ni-Mn-Ga have shown that the modulation is absent for structures with $c/a>1$.[13,14,21] Lanska *et al.* showed that for specimens with T_M between 325 and 355 K (or with e/a between 7.61 and 7.715), both the nonmodulated and a $5M$ modulated phase could coexist.[14] Above $T_M=355$ K (or $e/a=7.715$), the modulation is absent. In general, annealing of the powder removes the internal residual stress produced by mechanical grinding and results in sharpening of the Bragg peaks without any structural change. However, to study the possibility of structural change driven by the energetics, we have studied three compositions $x=0.2$, 0.26, and 0.35 after annealing at 500 °C for 10 h in high vacuum followed by cooling to RT. The XRD patterns before and after annealing the samples are shown in Fig. 7. As expected, all the Bragg peaks become sharper on annealing. Surprisingly, however, for $x=0.20$, additional reflections appear after annealing, suggesting an irreversible structural phase transition. The annealed pattern of $x=0.20$ can be indexed with respect to a monoclinic cell with lattice parameters $a=4.202$ Å, $b=5.497$ Å, and $c=29.341$ Å with $\beta=92.9°$. Since $c/a \approx 7$, the structure corresponds to the seven-layer modulated $7M$ phase. This $7M$ monoclinic structure for $x=0.2$ is different from that reported for the structure of the martensite phase of the stoichiometric composition Ni_2MnGa, which has orthorhombic symmetry.[7,16] These additional peaks are not observed for $x=0.35$ and are barely
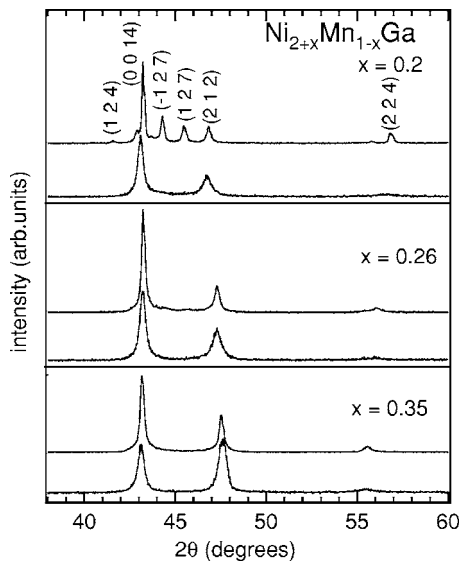
FIG. 7. Room-temperature x-ray diffraction pattern of Ni$_{2.2}$Mn$_{0.8}$Ga ($x=0.2$), Ni$_{2.26}$Mn$_{0.73}$Ga ($x=0.26$), and Ni$_{2.35}$Mn$_{0.66}$Ga$_{0.98}$ ($x=0.35$) before annealing (lower pattern) and after annealing at 500 °C for 10 h (upper pattern). The indices are with respect to a 7M monoclinic cell (see text).

visible for $x=0.26$, and the structure remains unchanged. This shows that for $x=0.35$ ($T_M=537$ K, $e/a=7.765$), the nonmodulated tetragonal phase is stable and is not affected by annealing. On the other hand, for $x=0.2$ ($T_M=334$ K, $e/a=7.65$), we obtain a structural transition in the martensitic phase from the nonmodulated to the 7M modulated phase at room temperature. This shows that although the composition is the same, the lattice constants might be different due to the appearance of modulation in the structure depending on the details of thermal history of the specimen. Conversion of nonmodulated to modulated crystal structure at room temperature has not been reported in literature so far.

D. Phase coexistence in Ni$_{2+x}$Mn$_{1-x}$Ga

The coexistence of phases, which is characteristic of first-order phase transition, is expected if the measurement temperature (300 K) lies in the hysteresis region. We indeed find that the austenitic and martensitic phases coexist at RT in the composition range $0.1 \leq x \leq 0.15$ (Fig. 5). The martensitic and austenitic peaks are marked in the $x=0.13$ XRD pattern, and the mole fraction of the martensitic phase is 36%. The percentage of the martensitic phase increases with x in the phase coexistence region from 24% ($x=0.1$) to 92% ($x=0.15$). For $x \geq 0.15$, the specimens are in fully martensitic phase.

DSC data for $x=0.13$ show that at RT the sample is not in fully austenitic phase, and this corroborates with the existence of the martensitic phase from XRD measurements (see the heating curve in Fig. 8). The transition temperatures (T_C and T_M), determined from DSC and χ_{ac}, are very sensitive to composition and increase with x (Table I). These are in agreement with the values reported in the literature and the recently published phase diagram of Ni$_{2+x}$Mn$_{1-x}$Ga.[8,11,12]
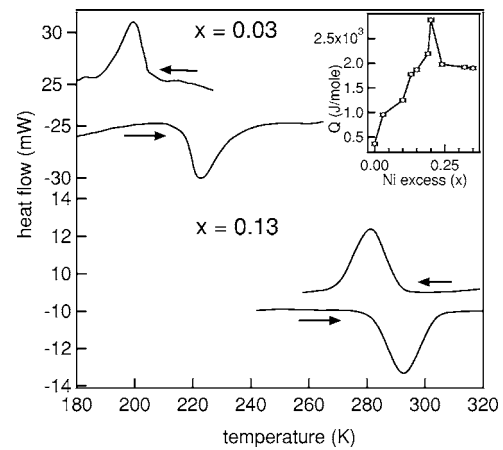

FIG. 8. The exothermic and endothermic heat flows for $x=0.03$ and 0.13; arrows indicate the heating and cooling directions. Inset shows the latent heat variation as a function of x.

The increase in the fraction of the martensitic phase with x and, finally, occurrence of the fully martensitic phase at RT can be explained by the increase of T_M with x. For $x=0.03$, DSC shows the hysteresis region to be well below RT and so the sample is in the austenitic phase. For $x=0.03$ (0.13), T_M, T_{M_f}, T_{A_s}, and T_{A_f} are 205 (292), 189 (270), 216 (281.5), and 234 (304) K, respectively. The width of hysteresis, which we define as the difference between $(T_{A_s}+T_{A_f})/2$ and $(T_M+T_{M_f})/2$,[12] turns out to be 28 K for $x=0.03$ and 11.8 K for $x=0.13$. The small width of hysteresis shows that the martensitic transition is truly thermoelastic, i.e., the driving force is small and the interface between the austenitic and martensitic phases is mobile upon heating and cooling. In the inset of Fig. 8, we show the latent heat variation as a function of x. For $x \leq 0.2$, the latent heat increases from 0.37 to 2.8 kJ/mole, as reported earlier.[10] Latent heat data for higher Ni compositions do not exist in literature. For $x=0.24$, the latent heat drops to 1.97 kJ/mole and decreases further for still higher compositions. This decrease in latent heat is related to the occurrence of the martensitic transition in the paramagnetic phase for $x \geq 0.24$.[12]

IV. CONCLUSION

We report the variation in crystal structure of Ni$_{2+x}$Mn$_{1-x}$Ga as a function of composition (x) at room temperature. The lattice constants of Ni$_{2.24}$Mn$_{0.75}$Ga have been compared with theoretical equilibrium lattice constants calculated by minimization of the total energy using full potential linearized augmented plane-wave (FPLAPW) method. The theoretically calculated lattice constants are in good agreement with the experimental values. This shows the reliability of density-functional theory based all-electron calculations using generalized gradient approximation to describe the structural properties of such complicated nonstoichiometric ternary alloys. In the composition range of $0.15 < x < 0.35$, a nonmodulated tetragonal martensitic phase is obtained, where with the increase in x, the unit cell is elongated along the c direction and compressed along the a and b axes.

The unit-cell volume decreases with increasing x. Increase in c/a with x results in the increase of strain by lattice distortion. Vegard's law is obeyed over this composition range. We find that annealing of $x=0.2$ specimen at 500 °C transforms the structure from the nonmodulated tetragonal phase to a $7M$ modulated monoclinic phase at RT. The coexistence of the austenitic and martensitic phases is observed at room temperature in the composition range of $0.1 \leq x \leq 0.15$. The fraction of the martensitic phase increases with x because of the increase in T_M. The small width of the hysteresis of the martensitic transition obtained from DSC shows its thermoelastic nature that is characteristic of a shape memory alloy.

*Electronic address: barman@csr.ernet.in

[1] S. J. Murray, M. Marioni, S. M. Allen, R. C. O'Handley, and T. A. Lograsso, Appl. Phys. Lett. **77**, 886 (2000).

[2] A. Sozinov, A. A. Likhachev, N. Lanska, and K. Ullakko, Appl. Phys. Lett. **80**, 1746 (2002).

[3] J. Marcos, L. Mañosa, A. Planes, F. Casanova, X. Batlle, and A. Labarta, Phys. Rev. B **68**, 094401 (2003).

[4] X. Zhou, W. Li, H. P. Kunkel, and G. Williams, J. Phys.: Condens. Matter **16**, L39 (2004).

[5] C. Biswas, R. Rawat, and S. R. Barman, Appl. Phys. Lett. **86**, 202508 (2005).

[6] P. J. Webster, K. R. A. Ziebeck, S. L. Town, and M. S. Peak, Philos. Mag. B **49**, 295 (1984).

[7] P. J. Brown, J. Crangle, T. Kanomata, M. Matsumoto, K.-U. Neumann, B. Ouladdiaf, and K. R. A. Ziebeck, J. Phys.: Condens. Matter **14**, 10159 (2002).

[8] A. N. Vasilev, A. D. Bozhko, V. V. Khovailo, I. E. Dikshtein, V. G. Shavrov, V. D. Buchelnikov, M. Matsumoto, S. Suzuki, T. Takagi, and J. Tani, Phys. Rev. B **59**, 1113 (1999).

[9] F. Albertini, L. Pareti, A. Paoluzi, L. Morellon, P. A. Algarabel, M. R. Ibarra, and L. Righi, Appl. Phys. Lett. **81**, 4032 (2002).

[10] V. V. Khovailo, V. Novosad, T. Takagi, D. A. Filippov, R. Z. Levitin, and A. N. Vasilev, Phys. Rev. B **70**, 174413 (2004).

[11] V. V. Khovaylo, V. D. Buchelnikov, R. Kainuma, V. V. Koledov, M. Ohtsuka, V. G. Shavrov, T. Takagi, S. V. Taskaev, and A. N. Vasiliev, Phys. Rev. B **72**, 224408 (2005).

[12] S. Banik, A. Chakrabarti, U. Kumar, P. K. Mukhopadhyay, A. M. Awasthi, R. Ranjan, J. Schneider, B. L. Ahuja, and S. R. Barman, Phys. Rev. B **74**, 085110 (2006).

[13] J. Pons, V. A. Chernenko, R. Santamarta, and E. Cesari, Acta Mater. **48**, 3027 (2000).

[14] N. Lanska, O. Söderberg, A. Sozinov, Y. Ge, K. Ullakko, and V. K. Lindroos, J. Appl. Phys. **95**, 8074 (2004).

[15] V. V. Martynov and V. V. Kokorin, J. Phys. III **2**, 739 (1992).

[16] R. Ranjan, S. Banik, S. R. Barman, U. Kumar, P. K. Mukhopadhyay, and D. Pandey, Phys. Rev. B **74**, 224443 (2006).

[17] V. V. Godlevsky and K. M. Rabe, Phys. Rev. B **63**, 134407 (2001).

[18] S. Fujii, S. Ishida, and S. Asano, J. Phys. Soc. Jpn. **58**, 3657 (1989).

[19] O. I. Velikokhatnyi and I. I. Nuamov, Phys. Solid State **41**, 617 (1999).

[20] A. Ayuela, J. Enkovaara, and R. M. Nieminen, J. Phys.: Condens. Matter **14**, 5325 (2002).

[21] C. Bungaro, K. M. Rabe, and A. Dal Corso, Phys. Rev. B **68**, 134104 (2003).

[22] S. R. Barman, S. Banik, and A. Chakrabarti, Phys. Rev. B **72**, 184410 (2005).

[23] V. A. Chernenko, V. A. L'vov, S. P. Zagorodnyuk, and T. Takagi, Phys. Rev. B **67**, 064407 (2003).

[24] J. Enkovaara, A. Ayuela, L. Nordström, and R. M. Nieminen, Phys. Rev. B **65**, 134422 (2002).

[25] J. Enkovaara, O. Heczko, A. Ayuela, and R. M. Nieminen, Phys. Rev. B **67**, 212405 (2003); J. Enkovaara, A. Ayuela, J. Jalkanen, L. Nordström, and R. M. Nieminen, Phys. Rev. B **67**, 054417 (2003).

[26] B. Wedel, M. Suzuki, Y. Murakami, C. Wedel, T. Suzuki, D. Shindo, and K. Itagaki, J. Alloys Compd. **290**, 137 (1999).

[27] J. M. MacLaren, J. Appl. Phys. **91**, 7801 (2002).

[28] A. Chakrabarti, C. Biswas, S. Banik, R. S. Dhaka, A. K. Shukla, and S. R. Barman, Phys. Rev. B **72**, 073103 (2005).

[29] R. A. Young, A. Sakthivel, T. S. Moss, and C. O. Paiva-Santos, *User's Guide to Program DBWS-9411* (1994).

[30] P. Blaha, K. Schwartz, and J. Luitz, *WIEN97* (Karlheinz Schwarz, Technical Universität, Wien, Austria, 1999).

[31] J. P. Perdew, K. Burke, and M. Ernzerhof, Phys. Rev. Lett. **77**, 3865 (1996).

[32] M. Weinert, E. Wimmer, and A. J. Freeman, Phys. Rev. B **26**, 4571 (1982).

[33] P. J. Brown, A. Y. Bargawi, J. Crangle, K-U. Neumann and K. R. A. Ziebeck, J. Phys.: Condens. Matter **11**, 4715 (1999).

[34] F. D. Murunagan, Proc. Natl. Acad. Sci. U.S.A. **50**, 667 (1944).

[35] A. Deb and Y. Sakurai, J. Phys.: Condens. Matter **12**, 2997 (2000).

[36] S. Picozzi, A. Continenza, and A. J. Freeman, Phys. Rev. B **66**, 094421 (2002).

[37] J. Zhu, X. W. Wang, and S. G. Louie, Phys. Rev. B **45**, 8887 (1992).

[38] J. P. Perdew, J. A. Chevary, S. H. Vosko, K. A. Jackson, M. R. Pederson, D. J. Singh, and C. Fiolhais, Phys. Rev. B **46**, 6671 (1992).

[39] B. L. Ahuja, B. K. Sharma, S. Mathur, N. L. Heda, M. Itou, A. Andrejczuk, Y. Sakurai, Aparna Chakrabarti, S. Banik, A. M. Awasthi, and S. R. Barman, Phys. Rev. B (to be published).

[40] L. Vegard, Z. Kristallogr. **67**, 239 (1928).

[41] A. R. Denton and N. W. Ashcroft, Phys. Rev. A **43**, 3161 (1991).

[42] X. Fan, T. Mashimo, X. Huang, T. Kagayama, A. Chiba, K. Koyama and M. Motokawa, Phys. Rev. B **69**, 094432 (2004).

[43] H. Saito, V. Zayets, S. Yamagata, and K. Ando, Phys. Rev. B **66**, 081201(R) (2002).

[44] J. Gallay, A. Deschanvres, S. Gaillard, and C. Alibert, Phys. Rev. B **11**, 5199 (1975).

[45] V. A. Chernenko, E. Cesari, V. V. Kokorin, and I. N. Vitenko, Scr. Metall. Mater. **33**, 1239 (1995).

[46] C. Jiang, G. Feng, S. Gong, and H. Xu, Mater. Sci. Eng., A **342**, 231 (2003).

[47] K. R. Priolkar, P. A. Bhobe, S. D. Sapeco, and R. Paudel, Phys. Rev. B **70**, 132408 (2004).